Pflugers Arch - Eur J Physiol (2014) 466:237–251
DOI 10.1007/s00424-013-1325-x

INTEGRATIVE PHYSIOLOGY

Genetic deletion of aquaporin-1 results in microcardia and low blood pressure in mouse with intact nitric oxide-dependent relaxation, but enhanced prostanoids-dependent relaxation

V. Montiel · E. Leon Gomez · C. Bouzin · H. Esfahani · M. Romero Perez · I. Lobysheva · O. Devuyst · C. Dessy · J. L. Balligand

Received: 26 May 2013 / Revised: 27 June 2013 / Accepted: 28 June 2013 / Published online: 20 July 2013

Abstract The water channels, aquaporins (AQPs) are key mediators of transcellular fluid transport. However, their expression and role in cardiac tissue is poorly characterized. Particularly, AQP1 was suggested to transport other molecules (nitric oxide (NO), hydrogen peroxide (H_2O_2)) with potential major bearing on cardiovascular physiology. We therefore examined the expression of all AQPs and the phenotype of AQP1 knockout mice (vs. wild-type littermates) under implanted telemetry in vivo, as well as endothelium-dependent relaxation in isolated aortas and resistance vessels ex vivo. Four aquaporins were expressed in wild-type heart tissue (AQP1, AQP7, AQP4, AQP8) and two aquaporins in aortic and mesenteric vessels (AQP1–AQP7). AQP1 was expressed in endothelial as well as cardiac and vascular muscle cells and co-segregated with caveolin-1. AQP1 knockout (KO) mice exhibited a prominent microcardia and decreased myocyte transverse dimensions despite no change in capillary density. Both male and female AQP1 KO mice had lower mean BP, which was not attributable to altered water balance or autonomic dysfunction (from baroreflex and frequency analysis of BP and HR variability). NO-dependent BP variability was unperturbed. Accordingly, endothelium-derived hyperpolarizing factor (EDH(F)) or NO-dependent relaxation were unchanged in aorta or resistance vessels ex vivo. However, AQP1 KO mesenteric vessels exhibited an increase in endothelial prostanoids-dependent relaxation, together with increased expression of COX-2. This enhanced relaxation was abrogated by COX inhibition. We conclude that AQP1 does not regulate the endothelial EDH or NO-dependent relaxation ex vivo or in vivo, but its deletion decreases baseline BP together with increased prostanoids-dependent relaxation in resistance vessels. Strikingly, this was associated with microcardia, unrelated to perturbed angiogenesis. This may raise interest for new inhibitors of AQP1 and their use to treat hypertrophic cardiac remodeling.

Keywords Aquaporins · Blood pressure · NO-dependent and independent endothelial function pathway · Prostaglandins

V. Montiel · E. Leon Gomez · C. Bouzin · H. Esfahani · M. Romero Perez · I. Lobysheva · C. Dessy (✉) · J. L. Balligand (✉)
Pole of Pharmacology and Therapeutics (FATH), Institut de Recherche Expérimentale et Clinique (IREC), Université catholique de Louvain, UCL-FATH Tour Vésale 5th floor 52 Avenue Mounier B1.53.09, 1200 Brussels, Belgium
e-mail: chantal.dessy@uclouvain.be
e-mail: jl.balligand@uclouvain.be

V. Montiel · O. Devuyst · J. L. Balligand
Department of Medicine, Cliniques Universitaires Saint-Luc, Brussels, Belgium

O. Devuyst
Pole of Nephrology (NEFR), Institut de Recherche Expérimentale et Clinique (IREC), Université catholique de Louvain, UCL-FATH Tour Vésale 5th floor 52 Avenue Mounier B1.53.09, 1200 Brussels, Belgium

Introduction

Aquaporins are transmembrane protein water channels involved in diverse physiologic functions in mammalians, including transepithelial fluid transport, brain water balance, cell migration with rapid changes in cell volume, cell proliferation, neuroexcitation, fat metabolism, or epidermal hydration [42]. Thirteen aquaporins are currently known (AQP0–AQP12) and

the first to be discovered by Agre and colleague in 1991 was AQP1 [34]—formerly called CHIP28. AQP1 protein is constitutively organized as a homotetramer where each monomeric subunit contains 269 amino acid residues and forms two tandem repeats of three-membrane-spanning α-helices, forming each six transmembrane domains (M1–M6) connected by five loops (loop A–loop E). Due to their repeated Asn-Pro-Ala consensus motif (also called NPA box), loop B (cytoplasmic) and loop E (extracellular) domains dip into the membrane and contribute to the central constriction site within the pore; the second aromatic/arginine, outer constriction site was later identified as a major contributor to selectivity in solute permeation through mutational analysis [3]. Each monomer works as an independent water pore but needs the tetrameric organization for proper functioning [50]. The intracellular loop D domain currently appears as a main gating domain for modulation of AQP1 activity via drugs interactions [48]. Some authors would attribute to AQP1 an additional role as a cGMP-gated cation channel and propose a five-pore model for the AQP1 homotetramere where cations would permeate AQP1 via a putative central pore with relative permeability of K^+, Cs^+, and Na^+ [5, 49]. However, this hypothetical cation permeability of AQP1 remains controversial [1, 43].

Some aquaporins, like AQP3, AQP7, AQP9, and AQP10 are also called "aquaglyceroporins" due to their capacity to transport small molecules like urea and glycerol [35]. Others are called unorthodox aquaporins, like AQP6, AQP8, AQP11, and AQP12, because of a highly conserved cysteine residue downstream of the second NPA box [21] whose function is currently being examined [35]. Finally, some authors have proposed that some aquaporins, including AQP1, would also transport other molecules besides water like CO_2, NH_3, and particularly nitric oxide (NO) [17, 18], although this remains debated. Some others authors have reported that AQP1 would also transport H_2O_2 [2].

The capacity to mediate transmembrane water transport justifies a particular interest for AQP1 in the heart, where myocardial edema is generated in many pathophysiologic conditions involving ischemia–reperfusion such as after an acute coronary occlusion or coronary artery bypass grafting. In basal situation, the passage of water is mainly done by diffusion and via aquaporins for only 28 %, but during osmotic stress (resulting, e.g., from metabolites accumulation in ischemic regions), water flow increases up to 800× mainly through AQP-mediated transport [22]. The impairment of myocardial function has been correlated with the presence of myocardial edema which could not only decrease systolic and diastolic function but also increase the diffusion distance of oxygen through thickened myocardial interstitium [10]. However, the specific implication of cardiac AQP1 in these phenomena is unknown.

Before examining the role of AQP1 in stressed conditions, one needs a full characterization of its function in cardiovascular homeostasis, as can be deduced from the phenotype of AQP1 knockout (KO) mice. In this study, we used mice with systemic deletion of AQP1 [24] and compared their phenotype to wild-type (WT) littermates of the same age. We focused on cardiac and vessel morphometry, histology, and blood pressure regulation by implanted telemetry. Moreover, we characterized the expression, cellular, and subcellular localization of AQP1 as well as other isoforms potentially upregulated in heart and vessels of AQP1 KO mice. We identified unexpected morphometric changes and abnormal endothelium- and prostanoids-dependent relaxation in AQP1 KO mice, which identify potential new roles of AQP1 in cardiovascular homeostasis. As new agonists and antagonists of this AQP are being developed [8], our observations raise interest for their use in cardiovascular diseases associated with heart and vessel remodeling.

Materials and methods

Animals

Breeding pairs of heterozygous aquaporin-1 KO mice in the Sv129 background were kindly provided by Dr. O. Devuyst (Division of Nephrology, Université catholique de Louvain, Belgium). Heterozygous mice were cross-bred to obtain homozygous AQP1 KO mice and their WT littermate controls. All studied mice were at least 16 weeks old and age-matched between genotypes. On the day of surgery, each mouse was anesthetized with ketamine hydrochloride (84 mg/kg; intraperitoneally (ip)) and xylazine hydrochloride (10 mg/kg, ip), and received analgesia after surgery (Buprenorphine 0.1-mg/kg, ip). All protocols were carried out in accord to the Guide for the Care and Use of Laboratory Animals published by the US National Institutes of Health.

Reverse transcriptase–quantitative polymerase chain reaction

All tissue extracts (fresh or directly preserved in RNA later (Ambion) at −80° C after sacrifice) were homogenized with tissue grinder using Trizol (Molecular Research Center) on ice. Purity and concentration of the RNA obtained was controlled by spectrophotometer (ND-1000 V3.7.1). The integrity of heart RNA was confirmed on agarose gels by the presence of 18S and 28S ribosomal RNA. After reverse transcription, real-time quantitative PCR (SYBR Green) was performed using an IQ5 multicolor Real-Time PCR detection system (Bio-Rad). Specific primer pairs for each aquaporin isoforms were used.[1] All reactions were run in triplicate, including negative controls without reverse transcriptase [28]. Results were expressed either as Ct (number of cycles needed to generate a fluorescent signal above a predefined threshold), ΔCt (corresponding to the difference between the Ct of the

[1] cf. Table 1

gene of interest and the Ct of the gene used to normalize the results), ΔΔCt (corresponding to the difference between the mean ΔCt of the gene of interest in the AQP1 KO genotype and the mean of ΔCt of this same gene in the WT control), or $2^{-\Delta\Delta Ct}$ (logarithmic value of ΔΔCt).

Antibodies

For western blot analysis, we used the following primary antibodies at the indicated dilutions: polyclonal rabbit anti-AQP1 (AB2219, Millipore, 1/5000), polyclonal goat anti-AQP4 (sc-9888, Santa Cruz Biotechnology, 1/500), polyclonal rabbit anti-AQP7 (ab32826, Abcam, 1/500), purified monoclonal mouse anti-AQP8 (AT1173a, Abgent, 1/1,000), polyclonal goat anti-COX-2 (sc-174, Santa Cruz Biotechnology, 1/250), polyclonal rabbit anti-caveolin-1 (610060, BD Biosciences, 1/10,000), and monoclonal mouse anti-β-actin (A5441, Sigma-Aldrich, 1/10,000). Secondary antibodies were all from Jackson ImmunoResearch (1:5,000). For immunohistochemistry, rabbit anti-AQP1 (Millipore, 1/1,000) and rat anti-CD31 (BD Biosciences, 1/50) were used and revealed with Alexa Fluor-conjugated secondary antibodies (Invitrogen, 1/500).

Ultracentrifugation protocol

Cardiac fresh tissues extracts were homogenized with tissue grinder, incubated in 1 ml of buffer solution containing Tris–HCl 20 mM (pH 7,4), dithiothreitol 0.1mM, saccharose 250 mM, and a mix of protease inhibitors (Sigma-Aldrich) 1/1,000 and fractionated by ultracentrifugation (105,000×*g* for 20 min at +4 °C). The supernatant (corresponding to soluble cytosolic extracts) was recovered and the pellet was suspended in 0.5 ml of buffer solution containing beta-glycerophosphate 80 mM, EGTA 20 mM, $MgCl_2$ 15 mM, Triton X-100 0.5 %, glycerol 10 %, and the same mix of protease inhibitors as mentioned above. After sonication and further centrifugation to remove cellular debris, the final supernatant (enriched in membrane fragments, including nuclei and cytoplasmic organelles) was recovered.

Western blot analysis

Denaturated proteins were loaded and separated on 15 % SDS-polyacrylamide gels (Mini-protean III, Bio-Rad) and transferred to a polyvinylidene difluoride membrane (PerkinElmer). After blocking with 5 % nonfat dry milk in Tris-buffered saline with 0.1 % Tween 20 (TBST, Sigma), membranes were incubated and hybridized with the antibodies cited above (overnight for all the primary antibodies except 1 h for β-actin), in TBST containing 1 % nonfat dry milk. After four washes (15 min each), membranes were incubated for 1 h with the respective secondary antibody in TBST containing 1 % nonfat dry milk. After four additional washes in TBST, membranes were incubated with a chemiluminescent reagent (ECL, Amersham for AQP1, AQP4, AQP8, caveolin-1, and β-actin, and Immobilon Western, Millipore for AQP7 and COX-2) and exposed to X-ray film.

Blood pressure and heart rate telemetry recording in vivo

Implants were surgically inserted as previously reported [7]. The use of miniaturized chronically implanted instruments with a recovery period of 10 days reduced the confounding effects of stress on the animals. Recordings were done during periods of 24 h to monitor circadian variations. The dose–response studies were performed via a chronically inserted intraperitoneal soft catheter connected to a syringe outside of the cage to avoid any stress to the animal. This catheter was gently removed from the animal after completion of the dose–response experiments.

Spectral analysis of systolic blood pressure and heart rate variability

Spectral analysis using a fast Fourier transformation algorithm on sequences of 512 points was performed using the HEM 3.4 software (Notocord Systems, France) on systolic blood pressure recordings in order to analyze the systolic blood pressure (and heart rate deduced from the tracings) variability (SBPV and HRV, respectively). The total spectral area of this variability can be subdivided into three specific known domains: the very low frequency ("VLF," between 0.05 and 0.4 Hz) of SBPV which is modulated by the NO-dependent endothelial function, the low frequency ("LF," between 0.4 and 1.5 Hz) of SBPV which reflects the sympathetic, and the high frequency ("HF," between 1.5 and 5 Hz) of HRV which is the parasympathetic regulation [33]. All values were normalized to the total spectral area from the same recordings in each mouse.

Myograph recording

Nineteen- to 20-week-old mice were euthanized and thoracic aortas were rapidly removed and immersed in ice cold physiological Tyrode solution (NaCl 128.3 mM, KCl 4.5 mM, $NaHCO_3$ 20.23 mM, NaH_2PO_4 0.35 mM, glucose 1 mM, $CaCl_2$ 1.35 mM, $MgSO_4$ 1.05 mM) gassed with a mixture of 95 % O_2–5 % CO_2. Vessel segments (<2 mm), cleaned of all fat and connective tissue, were mounted in a wire myograph M610 (DMT, Aarhus, Denmark). After normalization of the internal diameter, arterial rings were left to recover for 45–60 min. NO-mediated relaxation was evaluated in vessels precontracted with high KCl solution in presence of indomethacin 100 μM (NaCl 37.2 mM, KCl 95.6 mM, $NaHCO_3$ 20.23 mM, $NaH_2PO_4{\cdot}2H_2O$ 0.0546 mM, glucose 1.98 mM, $CaCl_2$ 1.35 mM, $MgSO_4$ 1.05 mM) and exposed to a dose–response of acetylcholine (10^{-8} to 3×10^{-5} M). In order to

analyze the participation of prostanoids in the endothelial relaxation, another set of experiments were performed following the same protocol but in the absence of indomethacin.

Myocytes and vessels immunohistochemistry

The hearts and vessels were dissected, embedded in Neg-50 frozen section compound (Microm), and subsequently frozen in liquid nitrogen vapors. Vessel cryosections (5 μm) were stained with hematoxylin and eosin. To quantify the cardiomyocyte area and the number of vessels, heart cryosections were labeled with rhodamine–wheat germ agglutinin (WGA), as a membrane marker, and with biotinylated-Isolectine B4, revealed with fluorescein–avidin, as an endothelial marker (all reagents from Vector). For AQP1 detection, vessel and heart cryosections were incubated with anti-AQP1 together with anti-CD31 antibodies or with fluorescein–WGA (Vector), respectively. Primary antibodies were revealed with AlexaFluor-conjugated antibodies as mentioned above. Nuclei were then stained with DAPI and labeled sections were imaged by structured illumination microscopy (Zeiss AxioImager equipped with an ApoTome module). Cardiomyocyte area was determined with Axiovision software.

Statistical analyses

All results are expressed as mean ± SEM. Raw data were first analyzed with a Kolmogorov–Smirnov test to confirm their normal distribution and then analyzed by Student's *t* test or two-way ANOVA where appropriate. The only exception was the analysis of vessels thickness where a nonparametric test (Mann–Whitney) was used. $P<0.05$ was considered statistically significant. Graph Pad Prism 4.0 was used to create the artwork.

Results

Identification and subcellular localization of aquaporin isoforms in cardiac and vascular tissues

Specific primers cited in Table 1 for all currently known aquaporins were used for reverse transcriptase–quantitative polymerase chain reaction (RTqPCR) in total extracts of the heart and aorta of WT mice from both genders. RTqPCR analysis of aquaporin transcripts, normalized to the best housekeeping gene tested of each organ (heart—HPRT, aorta—RPL13a), reveals the presence of a limited number of isoforms in the heart and in the aorta. Five aquaporin transcripts appeared to be expressed in the heart, namely, by order of abundance, AQP1, AQP7, AQP4, AQP8 and AQP11 (Fig. 1a, b). In the aorta, two aquaporins are expressed, namely, by order of abundance, AQP1 and AQP7 (Fig. 2a, b). Females had higher AQP1 expression in the heart than males ($P<0.05$; data not shown).

We next compared the abundance of these transcripts in AQP1 KO and their WT littermates using the $2^{-\Delta\Delta Ct}$ analysis to verify if AQP1 genetic deletion was accompanied with compensatory upregulation of the other aquaporin isoforms. We found that AQP4, AQP7, and AQP11 were significantly increased in the heart of male mice (Fig. 1c) but not in females, which exhibited a downregulation of AQP8 (Fig. 1d). In the aorta, no significant increases were observed (Fig. 2c, d).

We then used specific antibodies for these most abundant aquaporins to confirm their expression at the protein level in extracts of male heart, aorta, and mesenteric vessel from both genotypes (except for AQP11 for which specific antibodies are lacking). In WT mice, western blot analysis confirmed the presence of AQP1, AQP4, AQP7, and AQP8 in the heart (Figs. 1e and 3a) and AQP1 and AQP7 in the aorta (Figs. 2e and 3b) and in mesenteric artery (Fig. 2f). In AQP1 KO mice, we observed a significant upregulation of AQP4, AQP7, and AQP8 in the heart (Fig. 1f–h) and AQP7 in the aorta (Fig. 2g), but not in the mesenteric vessel (Fig. 2h).

We also resolved the subcellular localization of AQPs in heart tissue by ultracentrifugation and observed that AQP1 protein was located preferentially in the membrane compartments (Fig. 3a). For the remaining AQPs, subcellular localization varied among isoforms, with AQP7 showing the same subcellular distribution as AQP1 (Fig. 4b), but AQP4 being distributed both in the membrane and cytosolic fractions (Fig. 4a) and AQP8 preferentially in the cytosolic fraction (Fig. 4c). The comparison between genders also confirmed higher AQP1 expression in WT females (Fig. 3a) and lower AQP8 in AQP1 KO females consistent with our RTqPCR analysis.

Notably, we observed several bands for the AQP1 protein in total extracts of the heart (Fig. 3a), aorta (Fig. 3b), and mesenteric artery (Fig. 3c) which was attributed to differential migration of glycosylated proteins, as these disappeared after deglycosylation of both cardiac and aortic extracts (Fig. 3d).

AQP1 gene deletion results in abnormal heart and vessels morphometry

We analyzed the total heart as well as left ventricular (LV) weight/tibia length ratio in the two genders and genotypes. As illustrated in Fig. 5a–c, we observed microcardia in the AQP1 KO mice of both genders, as confirmed by lower values of LV weight/tibia length (4.8±0.13 vs. 5.8±0.15 in the WT, $n=16$ per genotype and gender; $P<0.001$). Histomorphometric analysis of cardiac myocytes transverse area confirmed significantly smaller myocytes in AQP1 KO (317.2 vs. 366.2 μm^2 in the WT, $n=6$ mice per genotype, 15 randomly chosen fields for each histologic section, and 9 histologic sections per heart, analyzed in blinded fashion, $P<0.001$; Fig. 5e), whereas capillary density was unchanged ($n=6$ mice per genotype, 15 randomly chosen fields for each histologic section, and 9

Table 1 Specifics primers used for each aquaporin isoform

	Forward oligonucleotide	Reverse oligonucleotide	Amplicon size (bp)
AQP0	5′-TTCAGCAACCACTGGGTGTA-3′	5′-CCATTGGAGTCACTGGGTCT-3′	140
AQP1	5′-GCTGTCATGTACATCATCGCCCAG-3′	5′-AGGTCATTGCGGCCAAGTGAAT-3′	107
AQP2	5′-GCCACCTCCTTGGGATCTAT-3′	5′-TGTAGAGGAGGGAACCGATG-3′	147
AQP3	5′-GGGGACCCTCATCCTTGT-3′	5′-AAGCCAAGTTGATGGTGAGG-3′	85
AQP4	5′-ATCCAGCTCGATCTTTTGGA-3′	5′-CTTCCTTAAGGCGACGTTTG-3′	156
AQP5	5′-TGGAGCAGGCATCCTGTACT-3′	5′-CGTGGAGGAGAAGATGCAGA-3′	151
AQP6	5′-CGGCCATGATTGGAACCTCT-3′	5′-AGCGGTCCTACCCAGAAGAT-3′	145
AQP7	5′-AGGCATGAACTCCGGATATG-3′	5′-CGGCTCTGAACACTTGTTTG-3′	98
AQP8	5′-TTGGGGCTCATCATTGCTAC-3′	5′-CCCTCCAAATAGCTGGGAGA-3′	138
AQP9	5′-TGGGGATTTGAGGTCCAC-3′	5′-GCTGGTTCTGCCTTCACTTC-3′	152
AQP10	5′-GGGGTTGCTTCCTAAGTGCT-3′	5′-GACAAAGGGAGGGGTCAGA-3′	151
AQP11	5′-AGCGCTCTACTGCACTTCCA-3′	5′-TTCGTCAAAGCACGGAAAGT-3′	156
AQP12	5′-AGCTCAACCCTGCGTACATC-3′	5′-TGCTGTGTAGGCCATGAGAG-3′	156

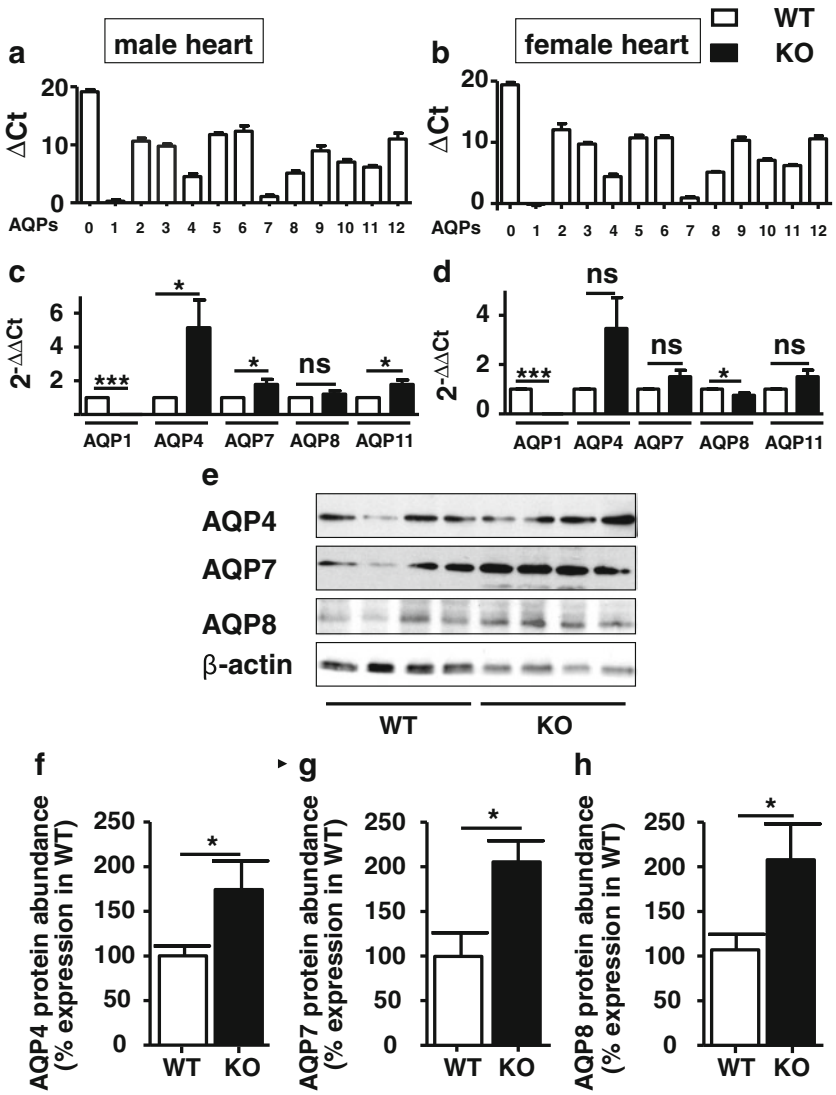

Fig. 1 Expression of AQP isoforms in cardiac tissue of WT and AQP1 KO mice. **a**, **b** Analysis of the relative expression of mRNA of AQP12 (expressed as ΔCt) in WT male (**a**) and female (**b**) mice (n=8 mice/group). AQP1, AQP4, AQP7 and AQP8 (with lower ΔCt) are the most abundant in cardiac extracts; **c**, **d** Comparative analysis of AQPs mRNA abundance in male (**c**) and female (**d**) AQP1 KO (*black bars*) and WT (*open bars*) mice (expressed as $2^{-\Delta\Delta Ct}$, relative to WT controls; n=8 mice per group), showing a relative upregulation of AQP4 and AQP7 in male AQP1 KO mice ; **e** Representative western blot of AQP4, AQP7, and AQP8 proteins in total extracts of hearts from AQP1 KO and WT male mice. Beta-actin signal is shown as loading control. The *bands* corresponding to the different AQPs isoforms migrated at 28 kDa and beta-actin at 43 kDa; **f**–**h** Quantification of the main cardiac AQPs proteins in AQP1 KO male mice, relative to basal expression in the WT (**f**: AQP4, **g**: AQP7, **h**: AQP8). Data were normalized to beta-actin. n=8 mice per group (except n=6 mice per group for AQP7). ***p<0.001, *p<0.05 and *ns*=not significant compared to WT mice

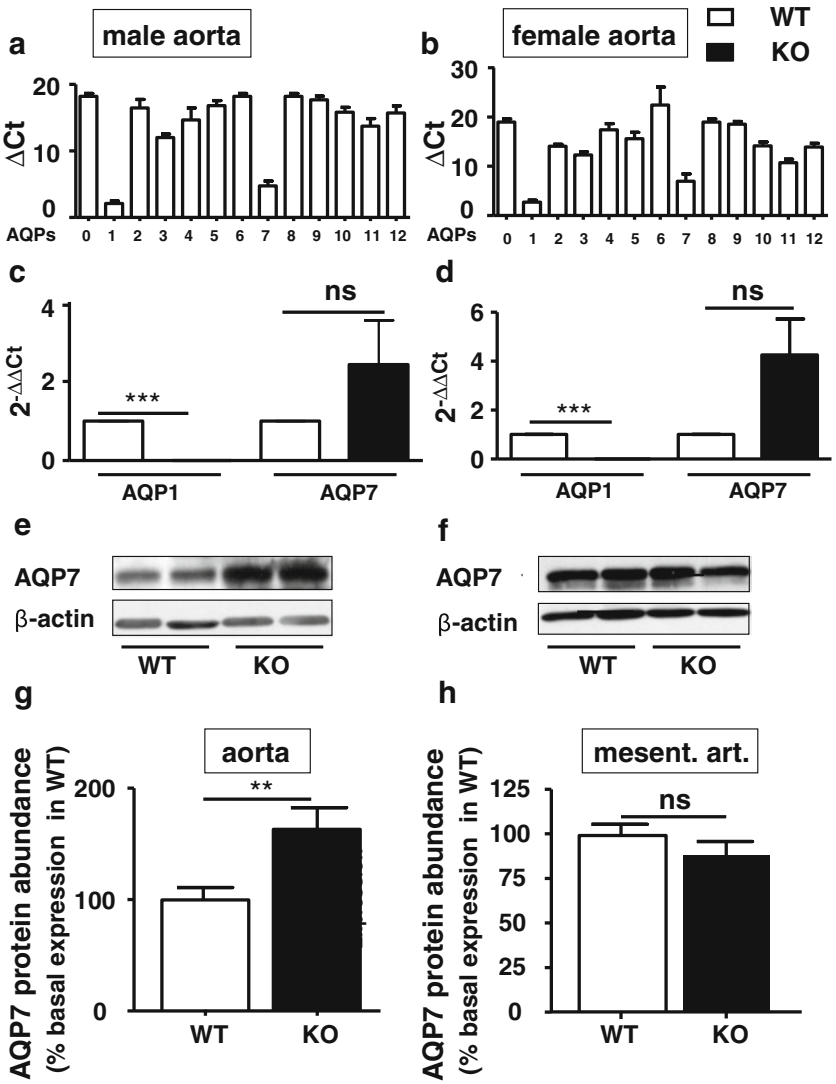

Fig. 2 Expression of AQP isoforms in aortic and mesenteric vessels of WT and AQP1 KO mice. **a**, **b** Analysis of the relative expression of mRNA of AQP0–AQP12 (expressed as ΔCt) in aortic extracts of WT male (**a**) and female (**b**) mice (n=5 mice/group). AQP1 and AQP7 (with lower ΔCt) are the most abundant in aorta. **c**, **d** Comparative analysis of AQPs mRNA abundance in the aorta of male (**c**) and female (**d**) AQP1 KO (*black bars*) and WT (*open bars*) mice (expressed as $2^{-\Delta\Delta Ct}$, relative to WT controls; n=5 mice/group); **e**, **f** Representative western blot of AQP7 proteins in total extract of aorta (**e**) and of mesenteric vessels (**f**) in AQP1 KO and WT male mice. Beta-actin signal is shown as loading control. The *bands* corresponding to AQP7 migrated at 28 kDa and beta-actin at 43 kDa; **g**, **h** Quantification AQP7 proteins in the aorta (**g**) and mesenteric vessels (**h**) from AQP1 KO male mice relative to WT controls. Data were normalized with beta-actin. n=12 mice per group for aorta and 9 mice per group for mesenteric vessels. ***p<0.001, **p<0.01 and *ns*=not significant compared to WT mice

histologic sections per heart, analyzed in blinded fashion, P=0.79; Fig. 5f). Figure 5d also illustrates the preferential localization of AQP1 in the cardiac myocyte membrane, consistent with our subcellular fractionation data (Fig. 3a).

Histomorphometric analysis of the vessels showed a significant decrease in the thickness of the arterial walls both in the aorta (Fig. 6a) and mesenteric artery (Fig. 6b) of the AQP1 KO mice from both genders (P<0.05 vs. WT for each vessel type; Mann–Whitney test). Figure 6c, d also shows the distribution of AQP1 staining both in the endothelium (co-staining with CD31) and medial smooth muscle cells of the WT vessel.

AQP1 KO mice exhibit lower blood pressure with preservation of circadian variation

We next measured the systolic, diastolic, and mean blood pressure of AQP1 KO mice and their WT littermate (from both genders) during 24 consecutive hours in non-anesthetized, awake mice under chronically implanted telemetry. We observed that AQP1 KO mice had a significantly lower systolic but no diastolic blood pressure with preservation of the circadian variation, in both genders (male, Fig. 7a; female, Fig. 7b). We also separately analyzed the recordings between nights and daylight hours (resting period for mice) in both genders and genotypes[2] which showed that the lower systolic and mean blood pressure in the AQP1 KO mice (of both genders) mainly occurs during the night (activity period for mice, Fig. 7c, d).

The hemodynamic profile of the AQP1 KO mice is not explained by dehydration

As systemic deletion of AQP1 is known to be associated with defective urinary concentrating ability and polyuria [24], we collected venous blood of AQP1 KO mice and their

[2] cf. Table 2

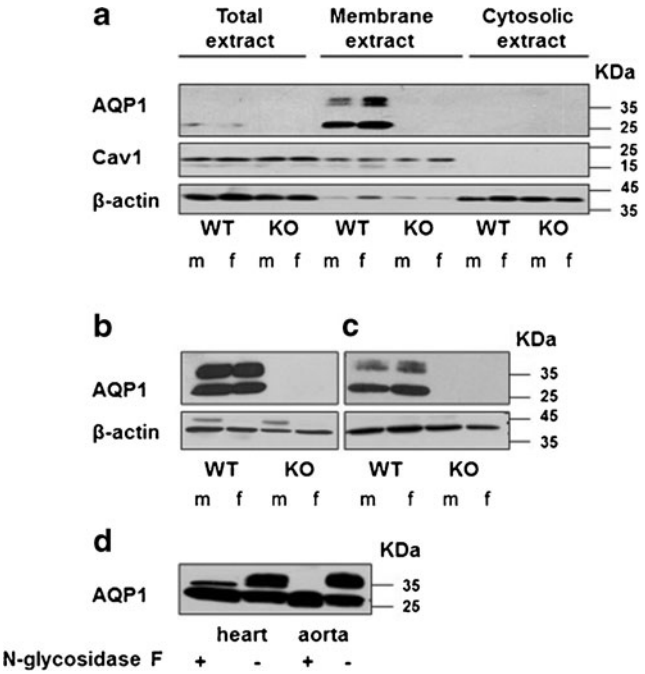

Fig. 3 AQP1 distribution in heart and vessels. **a** Subcellular compartmentation of AQP1 proteins in heart extracts. Representative western blot (of two experiments with similar results) of AQP1, caveolin-1 and beta-actin in total, membrane and cytosolic extracts of left ventricle of adult WT and AQP1 KO mice (male, *m*; and female, *f*) separated by ultracentrifugation. **b**, **c** AQP1 protein in aorta and mesenteric extracts. Representative western blot of AQP1 proteins in aorta (**b**) and mesenteric artery extracts (**c**) in adult WT mice and AQP1 KO mice (male, *m*; female, *f*). Beta-actin signal is shown as loading control. **d** AQP1 glycosylation in heart and aortic extracts from male mice. Representative western blot of AQP1 showing disappearance of additional upper bands after incubation with N-glucosidase F, indicative of AQP1 glycosylation

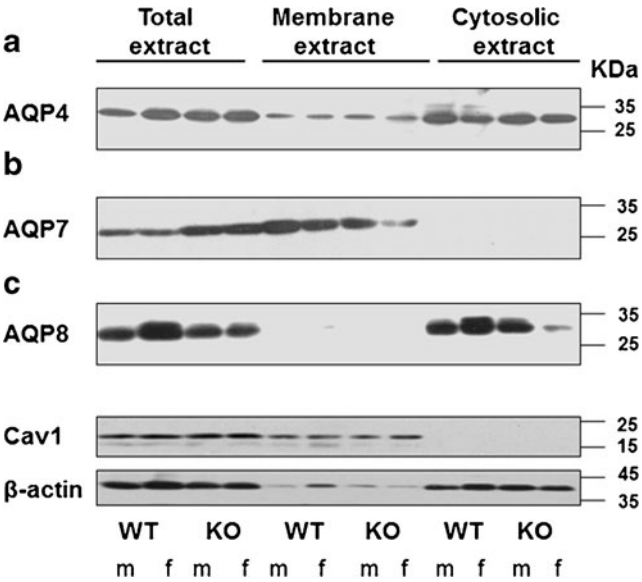

Fig. 4 Distribution of AQP4 (*a*), AQP7 (*b*), and AQP8 (*c*) in the adult male and female heart. Representative western blot (of two experiments with similar results) of AQP4 (*a*), AQP7 (*b*), and AQP8 (*c*) in total, membrane, and cytosolic extracts of left ventricle of adult WT and AQP1 KO mice (male, *m*; female, *f*) separated by ultracentrifugation. The same filter as in Fig. 3 was stripped and reprobed thereby showing the same signals for caveolin-1 and beta-actin for comparison

WT littermate (both genders) at the time of sacrifice and analyzed biological markers. The results confirmed the similar water balance in these mice.[3] Nevertheless, we observed a statistical difference in the daily water intake between the two genotypes (AQP1 KO mice, 10.9±0.9 vs. 5.6±0.6 ml in the WT group, $P<0.001$), suggesting that AQP1 KO mice may have compensated urinary water loss by increased drinking.

Spectral analysis of systolic blood pressure variability shows preserved control by the autonomic nervous system and the NO pathway in AQP1 KO mice

We first compared the spectrum of the SBPV or HRV of AQP1 KO mice and their WT littermate (both genders) in the three frequency domains (VFL, LF, and HF) and did not observe any difference between the two genotypes,[4] particularly in the VLF domain reflective of NO-dependent regulation (Fig. 8b). To refine the analysis of the NO pathway, similar measurements were repeated after treatment with the NOS inhibitor, L-NAME. NOS inhibition raised mean blood pressure (MBP) to a similar value in both genotypes (Fig. 8a). Similarly, L-NAME increased SBPV in the VLF in both genotypes (Fig. 8c), suggesting preserved function of the endogenous NO pathway in both genotypes.

To test the sensitivity of downstream NO targets, graded doses of an exogenous NO donor (sodium nitroprusside) were infused through chronically implanted intraperitoneal catheters in telemetered mice. Sodium nitroprusside dose-dependently and identically reduced the SBPV in both genotypes (Fig. 9a). To avoid any interference from endogenous NO, measurements were repeated after NOS inhibition with L-NAME. The initial administration of L-NAME (30 min) identically increased the variability, as expected, after which increasing doses of sodium nitroprusside again reduced SBPV identically in both groups (Fig. 9b). This suggested preserved sensitivity to both endogenous and exogenous NO in the vasculature of both genotypes.

Consistent with an intact autonomic control, we also observed a preserved baroreflex response in the AQP1 KO mice, i.e., a decrease of heart rate proportional to blood pressure increases following administration of the vasoconstrictor, phenylephrine, which was comparable to WT (P=ns; two-way ANOVA for paired data; WT, Fig. 9c; AQP1 KO, Fig. 9d).

[3] cf. Table 3
[4] cf. Table 4

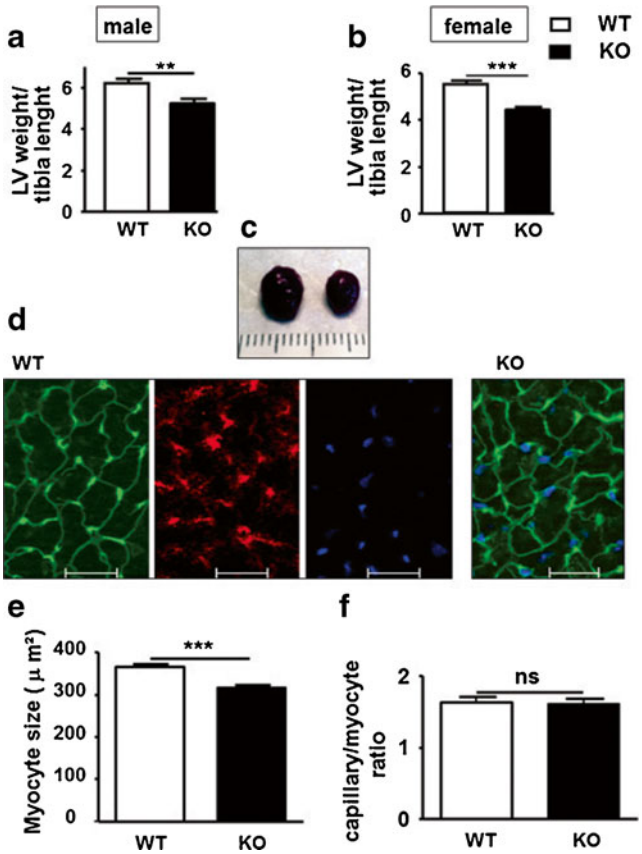

Fig. 5 Comparative cardiac morphometry shows microcardia in AQP1 KO mice compared with WT littermates. **a**, **b** Left ventricular (LV) weight normalized to tibia length in adult male (**a**) and female (**b**) WT (*open bars*) and AQP1 KO (*black bars*) of the same age (n=16 per genotype and gender); **c** representative gross morphology of a heart from a WT (*left*) and an AQP1 KO mouse (*right*) (*scale bar* in millimeter); **d** WGA staining (*green*, membrane), AQP1 immunofluorescence (*red*), DAPI staining (*blue*), and merged image in a WT heart cryosections and merged image in a KO heart cryosections (*scale*, 20 μm). **e**, **f** Myocyte transverse area (**e**) and capillary density (**f**) in cardiac sections from WT and AQP1 KO mice (n=6 in each genotype). Mean values (±SEM) were calculated from measurements in 15 randomly chosen fields for each histologic section (nine histologic sections per heart, analyzed in blinded fashion). ***p<0.001, **p<0.01, and *ns* = not significant compared to WT mice

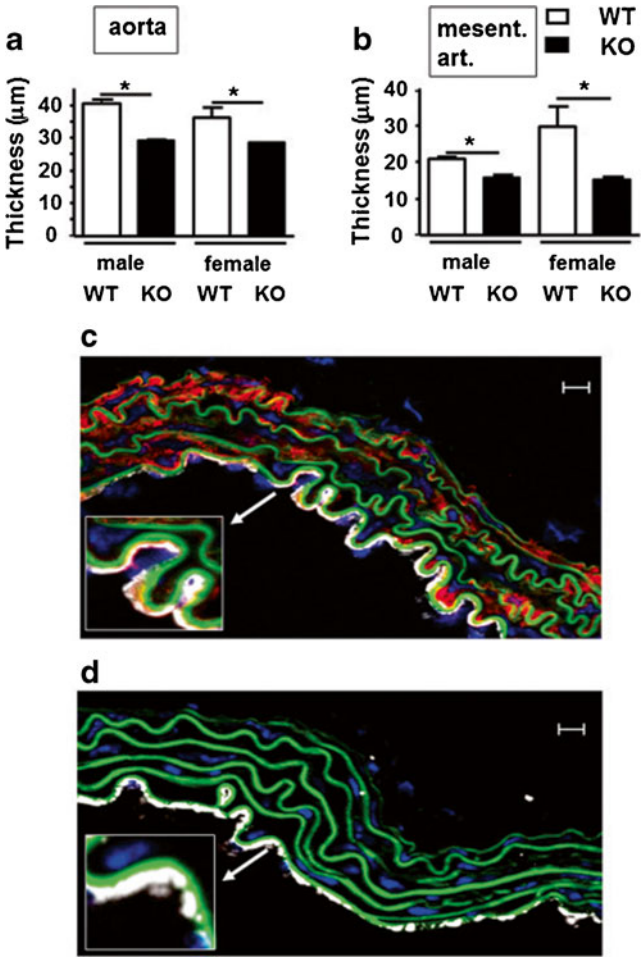

Fig. 6 Vessels morphometry in AQP1 KO mice compared with WT littermates. **a**, **b** Comparative vessels morphometry shows thinner vessel walls in AQP1 KO mice compared with WT littermates. Vessel thickness of aorta (**a**) and mesenteric artery (**b**) in WT and AQP1 KO mice (n=3 for each genotype and gender). Mean values (±SEM) of thickness were measured on four different points for each vessel (four histologic sections per vessel, analyzed in blinded fashion). *p<0.05 compared with WT mice (Mann–Whitney test). **c**, **d** Hematoxylin and eosin staining of aortic rings in WT (**c**) and AQP1 KO mice (**d**), showing co-staining (in WT) for AQP1 in *red* and CD31 in *white* (*scale bar*, **10 μm)**

Ex vivo analysis of vascular reactivity shows unchanged NO-dependent relaxation in aortic and mesenteric rings from AQP1 KO mice, but a potentiation of the prostanoids-dependent relaxation

We further analyzed the endothelial NO-dependent relaxation in aortic and mesenteric rings of male AQP1 KO and their littermate WT.

First, aortic and mesenteric rings were precontracted with KCl (50 mM) in presence of indomethacin (100 μM) and a dose–response curve to acetylcholine (Ach) (10^{-8} to 3×10^{-5} M) was performed to analyze the NO-dependent relaxation. The results do not show any statistical difference between genotypes (Fig. 10a, c). To evaluate dual effects of NO and endothelium-derived hyperpolarizing factor (EDH(F)) in endothelial-dependent relaxation to Ach, aortic and mesenteric rings were preconstricted with phenylephrine (3 μM) (in the presence of indomethacin). Again, no difference in relaxation was observed (Fig. 10b, d).

We next analyzed similar dose–response curves to Ach in aortic and mesenteric rings precontracted with KCl (50 mM) but in the absence of indomethacin to preserve the prostanoids-dependent relaxation in addition to NO. In the aorta of AQP1 KO mice, this resulted in a potentiation of the Ach relaxant effect at low concentrations (up to 3×10^{-7} M), which was reversed at higher concentrations (Fig. 11a). In mesenteric vessels, however, the relaxant response was

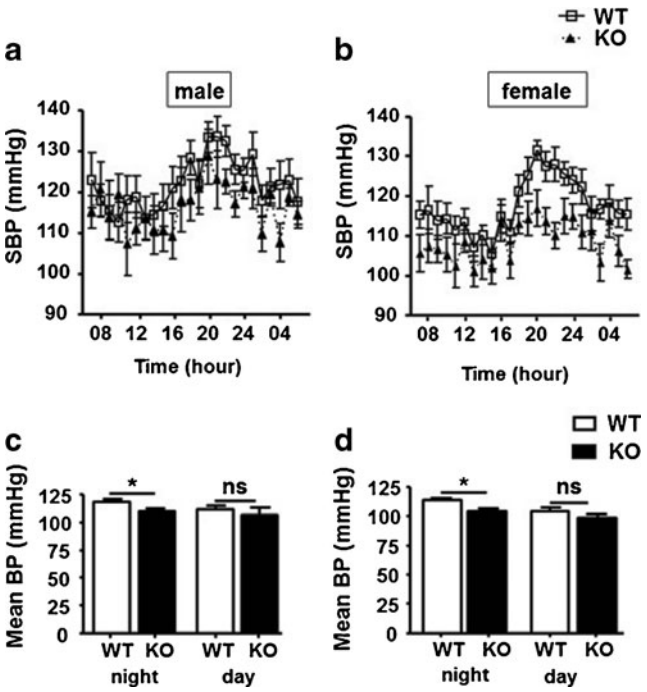

Fig. 7 Circadian variation of systolic blood pressure in WT and AQP1 KO mice. **a**, **b** Blood pressure was recorded by telemetry for 24 h in male (**a**) and female (**b**) WT (*open squares*) and AQP1 KO mice (*filled triangles*); (**a**, n=8 WT and 5 KO; **b**, n=8 WT and 6 KO). Mean values (±SEM) of SBP were calculated for each 60-min sequence of recording. A significant effect related to genotype was confirmed by two-way ANOVA in each gender. **c**, **d** Mean blood pressure (MBP) in WT (*open bars*) and KO mice (*black bars*) from both genders (**c**, male; **d**, female). Blood pressure was recorded over 24 h, separated in two sequences of 12 h recording (night and day). Mean values (±SEM) of MBP were calculated for each 12 h sequence of recording. *p<0.05 and *ns* = not significant compared with WT mice

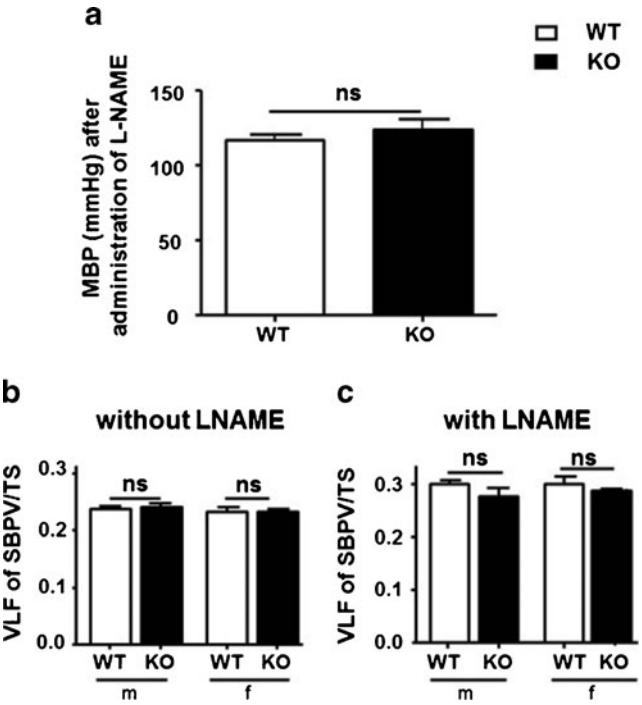

Fig. 8 Comparative effects of nitric oxide synthase (NOS) inhibition on blood pressure in AQP1 KO and WT littermates. **a** MBP observed under telemetry in WT (*open bars*) and AQP1 KO mice (*black bars*) after L-NAME administration, n=6 per genotype. **b**, **c** Spectral analysis of systolic blood pressure variability (SBPV) in the very low frequency domain (VLF) reported to total spectral area (TS) in WT and AQP1 KO mice (male, *m*; female, *f*) before (**b**) and after L-NAME administration (**c**). Mean values (±SEM) of SBPV were calculated for each 60-min sequence of recording, during 24 h in WT mice (without L-NAME: n=15, 8 m and 7 f. with L-NAME: n=9, 5 m and 4 f. and AQP1 KO mice (without L-NAME: n=15, 8 m and 7 f. with L-NAME: n=9, 5 m and 4 f). L-NAME was given in the drinking water at the concentration of 2 mg/ml during seven consecutive days. *p<0.05 and *ns* = not significant compared to WT mice

significantly potentiated up to 3×10^{-6} M, with maximal relaxation identical to WT (Fig. 11b).

To examine the potential source of such enhanced prostanoids response, we first measured the abundance of transcripts for the two cycloxygenase isoforms (COX-1 and COX-2) in extracts of aortic and mesenteric arteries. Only COX-2 could be amplified from these vessels (data not shown). We then performed a western blot analysis of total extracts of the same vessels using a specific antibody against COX-2. In the aorta, we did not find any difference in terms of protein expression between the two genotypes (Fig. 11c, e). However, in mesenteric vessels, COX-2 expression was significantly higher in the AQP1 KO compared to the littermate WT (Fig. 11d, f).

Discussion

The expression of the water channels, aquaporins, has been demonstrated in hearts from humans, rats, and mice and AQP1 appears as the most abundant aquaporin in all these species [4].

Indeed, our expression analysis in WT mice shows AQP1 to be highest, followed in order of abundance by AQP7, AQP4, AQP8, and AQP11. In cardiac extracts, we found AQP1 to be predominantly expressed in membrane fractions and to be glycosylated, as in other tissues [6, 27]. Our immunohistochemical analysis reveals AQP1 expression both in cardiac endothelial cells and myocytes, consistent with previous observations (including by electron microscopy [32]). Likewise, AQP1 was not only clearly identified in endothelial cells of aortic vessels but also in vascular smooth muscle cells of the aortae and first- and second-order mesenteric arteries. Likewise, AQP1 expression had been shown in rat pulmonary artery [23] and in human coronary artery where it mediated rapid water transport in response to changes in external osmolarity [39].

As the purpose of our study is to characterize the role of AQP1 on the cardiovascular phenotype in AQP1 KO mice,

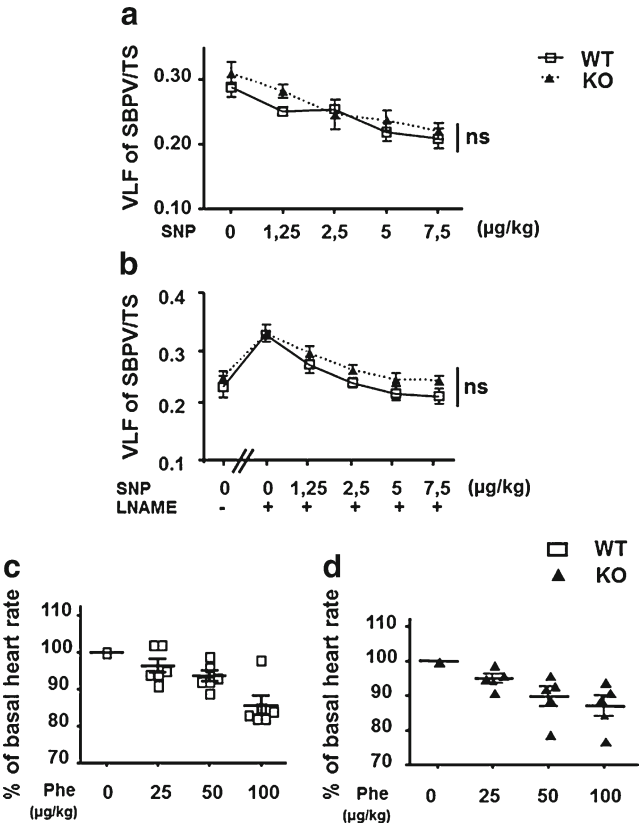

Fig. 9 Deletion of AQP1 does not affect the BP variability or baroreflex response to a NO donor in vivo. **a**, **b** Decrease of the systolic blood pressure variability (SBPV) in the very low frequency domain (VLF) reported to total spectral area (TS) under increasing doses of sodium nitroprusside (NO donor), administered alone (**a**) and under L-NAME (30 mg/kg; ip, **b**), in WT (*open squares*) and AQP1 KO mice (*filled triangles*) under telemetry (n=6/mice per group). Mean values (±SEM) of VLF of SBPV were calculated during each dose response sequence of recording. **c**, **d** Baroreflex response in WT (**c**) and AQP1 KO mice (**d**) under telemetry. Percent decrease from basal heart rate correlates with graded administration of phenylephrine (from 25 to 100 µg/kg). Each values of HR were calculated during each dose–response sequence of recording

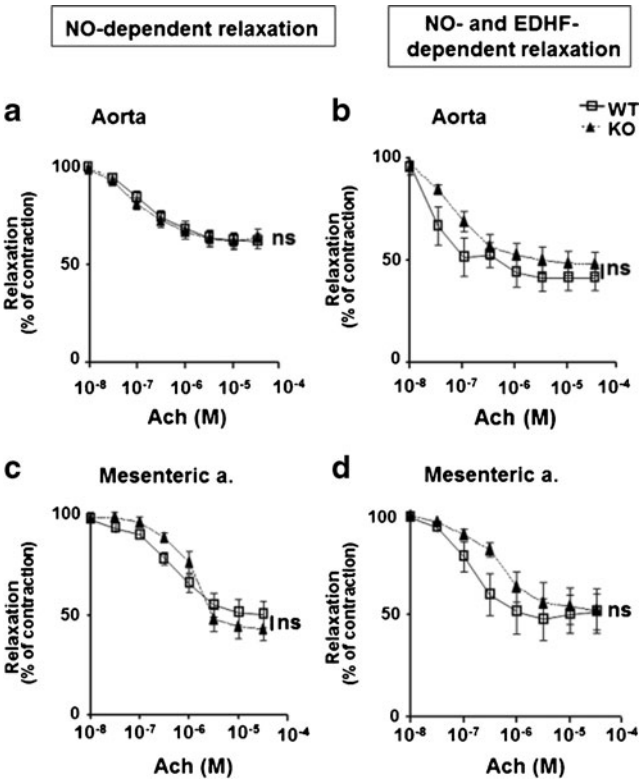

Fig. 10 Deletion of AQP1 does not affect the NO and EDH relaxations in aortic and mesenteric vessels. **a**, **d** Endothelium-dependent relaxation in aortic rings (**a**, **b**) and mesenteric artery rings (**c**, **d**) from WT (*open squares*) and AQP1 KO (*filled triangles*) male mice. Rings were precontracted with 50 mM KCl in the presence of indomethacin (100 µM) and a dose–response curve to acetylcholine (Ach) (10^{-8} to 3×10^{-5}M) was performed to analyze the nitric oxide (NO)-dependent relaxation in rings from WT and KO mice (**a**, **c**). To evaluate the dual effect of NO and EDHF in acetylcholine-induced relaxation, rings were preconstricted with phenylephrine 3 µM (**b**, **d**). Results are expressed as means±SEM from measurements on four rings per mouse (n=4 WT and 4 KO mice in **a**, **b** and n=5 WT and 5 KO in **c**, **d**). *ns* = not significant compared to WT

we first examined whether deletion of this isoform affects the expression of other aquaporins. Indeed, we found overexpression of AQP4, AQP7, and AQP8 in the hearts of male AQP1KO mice (Fig. 1e–h), but only AQP7 in their vessels (Fig. 2e–h). AQP4 protein expression was previously shown in cardiac tissue of different species [4, 36], although this isoform has been mainly implicated in development and resolution of brain edema [37]. However, its role can probably be extended to the control of myocardial edema since it was shown to be upregulated with cell swelling in a murine model of myocardial infarction [46] and infarct size was reduced in AQP4 KO mice after coronary artery ligation [36]. This would be consistent with its partial localization at cardiac membranes, as observed in our study (Fig. 4a). AQP8 transcripts had previously been detected in the heart (but the protein was not detected probably due poor performance of antibodies [4, 25]). Although AQP8 expression is extensively described in the gastrointestinal tract including in hepatocytes and Kupffer cells [20], its role in the heart remains unclear. In primary cultures of hepatocytes, AQP8 was present in intracellular vesicles, with increased plasma membrane trafficking upon stimulation with cAMP [14]. Likewise, our fractionation experiments show an exclusive localization in cytosolic extracts (Fig. 4c), but whether a similar redistribution can be induced upon stimulation is unknown. AQP7 has the same subcellular distribution as AQP1 in our hands, i.e., it co-localizes with caveolin-1 in membrane extracts (Fig. 4b). So far, only the AQP7 transcripts had been detected in cardiac tissue [19] and AQP7 protein had been shown by immunohistochemistry in capillaries [40] or in skeletal muscle cells [44]. This is of particular interest in light of its known implication in the transport of glycerol from the bloodstream through the endothelial (and probably myocyte) membranes. Recent evidence

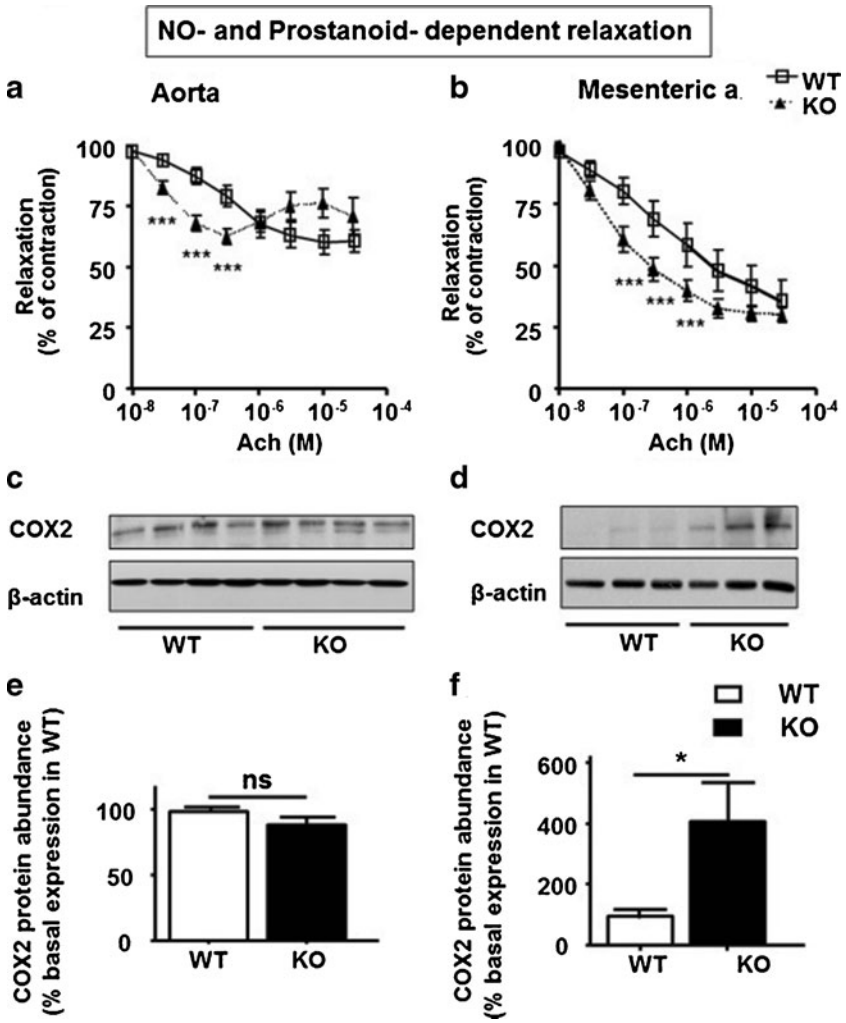

Fig. 11 Deletion of AQP1 results in potentiation of prostanoids-dependent relaxation, correlated with increased COX-2 in resistance vessels. **a**, **b** NO- and prostanoids-dependent relaxation in aortic (**a**) and mesenteric rings (**b**). Rings were precontracted with 50 mM KCl in absence of indomethacin and acetylcholine (Ach) dose–response curve (10^{-8} to 3×10^{-5} M) was performed to analyze the effect of nitric oxide (NO) and the prostanoids pathway on the relaxation of rings from WT (*open squares*) and AQP1 KO mice (*filled triangles*). Results are expressed as means±SEM from measurements on four rings per mouse ($n=8$ mice per genotype in **a** and $n=6$ mice per genotype in **b**). **c**, **d** Representative western blot (of two experiments with similar results) of COX-2 proteins in total extract of aorta (**c**) and of mesenteric vessels (**d**) in AQP1 KO and WT male mice. Beta-actin signal is shown as loading control. The *bands* corresponding to COX-2 migrated at 70 kDa and beta-actin at 43 kDa. **e**, **f** Quantification of COX-2 proteins in aorta (**e**) and mesenteric extracts (**f**) in AQP1 KO mice (*black bars*) relative to abundance in WT mice (*open bars*). Data were normalized to beta-actin ($n=8$ mice/genotype for **e** and $n=4$ mice/genotype for **f**) ***$p<0.001$, *$p<0.05$, and *ns* = not significant compared to WT mice

implicates glycerol not only as an energetic substrate but also a key regulator of lipid metabolic pathway influencing the balance of glucose/fatty acid utilization in the heart. Although the cardiac muscle cell mainly utilizes fatty acids as an energy source in physiologic conditions [29], increasing glycerol availability shifts the balance towards to an increase in glucose utilization resulting in a reduced oxygen consumption and β-oxidation of lipids, a simultaneous increase of phospholipid (instead of triglycerides) synthesis into the myocyte membrane leading to cardiac cytoprotection [12]. Accordingly, AQP7 KO mice did not adapt well to pressure overload with an increase in mortality rate after transverse aortic constriction [19]. Whereas the contribution of glycerol as energetic substrate is probably low in resting conditions (15 % of glucose oxidation [12] but can sustain heart beating ex vivo as sole substrate [19]), it could significantly increase under stress, as modeled by catecholamine-induced tachycardia [13]. Therefore, upregulation of AQP7 may be cardioprotective. However, the functional significance of AQP7 expression in the aorta and mesenteric vessels, as clearly shown in our study (Fig. 2a, b, e, f), remains speculative, as glycerol is not used as energetic substrate in these vessels, at least according to conventional thinking. It may, however, impact on glycerol transport to or from periadventitial fat, which may influence triglycerides

Table 2 Hemodynamic profile of the two genotypes in both genders

	WT mice		KO mice		*P* value	
	Male (n=7)	Female (n=8)	Male (n=6)	Female (n=6)	Male (WT vs. KO)	Female (WT vs. KO)
SBP 24 h	125.6±3	119.3±2	117.1±2	109.2±2	ns	*
DBP 24 h	104.4±4	98.4±3	95.6±3	92.9±3	ns	ns
MBP 24 h	115.1±3	109.7±2	106.6±3	101.7±2	ns	*
SBP 12 h (night)	128.8±2	123.8±2	120.2±2	111.8±2	*	**
DBP 12 h (night)	107.4±3	101.9±2	98.15±4	95.51±3	ns	ns
MBP 12 h (night)	118.3±3	113.4±3	109.5±3	104.3±3	*	*
SBP 12 h (day)	121.3±3	113.8±3	113.7±3	106.2±3	ns	ns
DBP 12 h (day)	100.3±3	93.2±3	92.6±5	89.6±3	ns	ns
MBP 12 h (day)	111.5±3	104.2±3	103.4±4	98.5±4	ns	ns

Blood pressures were expressed in millimeter of Hg and were obtained in chronically telemetered mice. Data are mean±SEM

SBP systolic blood pressure, *DBP* diastolic blood pressure, *MBP* mean blood pressure, *ns* not significant compared to WT mice

*p<0.05; **p<0.01 (compared to WT mice)

accumulation in adipocytes and their ensuing production of inflammatory cytokines. Whether these phenomena are implicated in the development of neoadventitia and atherosclerosis remains to be proven [15, 26].

Compared with age-matched WT littermate, we confirmed that AQP1 KO mice had lower blood pressure, as previously observed [30]. However, our use of chronically implanted telemetry in unanesthetized mice allowed a more complete analysis of short- and long-term variability as well as autonomic control. Indeed, our analysis shows that the reduced mean blood pressure in AQP1 KO is mainly due to a decrease in systolic (not diastolic) BP during the night (i.e., activity period for mice; Fig. 7a, b and Table 2). As AQP1 KO mice are known to exhibit mild polyuria and could present defective water balance, we measured biological parameters before sacrifice; as shown in Table 3, the values (hematocrit, BUN, creatinine, and plasma osmolality) do not confirm dehydration. This is probably explained by a compensatory increase in water intake, as confirmed by our measurements. Together with our observation of systolic (not diastolic) low BP only during the night, these measurements reasonably exclude dehydration as a likely cause for hypotension.

Given the uncertainty about the aetiology of this arterial hypotension, we decided to study in more detail the neurohormonal regulation of AQP1 KO mice by spectral analysis of blood pressure variability (as previously done by us in mice [7]). The total spectra area of BP and HR variability can be subdivided into three specific known domains: the very low frequency (VLF, between 0.05 and 0.4 Hz) of SBPV which is influenced by the NO-dependent endothelial function, the low frequency (LF, between 0.4 and 1.5 Hz) of SBPV which reflects the sympathetic modulation, and the high frequency (HF, between 1.5 and 5 Hz) of HRV which is the parasympathetic pathway [7] (Table 4). No difference was observed in terms of sympathetic nervous system balance between the two genotypes[5] which could therefore not explain the difference in hemodynamic profile observed; in particular, AQP1 KO mice exhibited a normal baroreflex arc, with a reduction in HR proportional to vasoconstrictor-induced increase in BP, and a slope identical to WT littermates (Fig. 9c, d).

Since the endogenous NOS system is a key regulator of BP, we studied the response of these mice to NOS inhibition in vivo. L-NAME increased MBP to a similar value in both genotypes (Fig. 8a). Specific analysis of the NO-sensitive VLF revealed identical values in both genotypes (and genders) at baseline and a similar increase after L-NAME (Fig. 8b, c). These results are consistent with a preserved NO-dependent endothelial function pathway in the AQP1 KO mice in vivo. Furthermore, the preservation of the VLF response to exogenous NO (before and after endogenous NOS inhibition) rules out any alteration in downstream response of the NO pathway (Fig. 9a, b). Finally, the integrity of endothelial and NO-mediated relaxation was confirmed in isolated aortic and mesenteric rings ex vivo, after precontraction with KCl and indomethacin treatment to exclude EDH(F) and prostanoids involvement, respectively.

This is in contrast [17] with previous reports of impairment of the endothelial NO-dependent relaxation in aortic rings of AQP1 KO mice. Several explanations may account for this difference. Unlike in our study, true littermate control mice were not used in this earlier report (CD1 mice were used as control group) while endothelial NO-dependent relaxation is known to vary between different strains (as confirmed by an independent comparison between Sv129 and

[5] cf. Table 4

Table 3 Biological values of WT and AQP1 KO mice

	WT mice (n=22)	KO mice (n=16)	P value
Hematocrit (%)	40±0.7	41±0.7	ns
Osmolality (mOsm/kg)	340.6±6.1	340.7±4.8	ns
Urea (mg/dl)	53.7±2.32	46.9±2.64	ns
Creatinine (mg/dl)	0.22±0.05	0.13±0.01	ns
Water intake (ml/day)	5.6±0.5	10.9±0.6	***

Hematocrit, osmolality, urea, and creatinine values were taken from venous blood samples. Data are mean±SEM

ns not significant compared to WT mice

***p<0.001 (compared to WT mice)

C57BL6/J in our lab; data not shown). Also, pretreatment with indomethacin (known to inhibit COX-dependent production of prostanoids [16]), was not included in the protocols of this earlier study so that some of these observations could have resulted from an endothelial prostanoids-dependent response superimposed on NO.

Since the NOS-dependent response is unperturbed in AQP1 KO compared with WT littermate, we examined NOS-independent endothelial responses. We found no difference in ex vivo relaxation with superimposed EDH(F) response (Fig. 10b, d), but a phenotype was clearly apparent when EDH(F) was excluded (with KCl precontraction) but prostanoids were preserved (in absence of indomethacin; Fig. 11a, b); this resulted in a bimodal relaxation in the aorta with early potentiation that was reversed at higher agonist concentration (Fig. 11a); this was probably due to concentration-dependent release of relaxant and contracting prostanoids in response to Ach in the aorta. In resistance (mesenteric) vessels of AQP1 KO, however, a unimodal potentiation of the relaxation was observed (Fig. 11b). As we did not find COX-1 transcripts (by RTqPCR) in aortic as well as in mesenteric artery extracts in either mouse strain, we postulated that COX-2 was the major cyclooxygenase involved in prostanoids production in these vessels. Consistent with enhanced prostanoids-dependent relaxation, we found increased COX-2 proteins in mesenteric (but not aortic) extracts of AQP1 KO mice. Together with unperturbed NO and EDH(F) relaxations, the fact that indomethacin (a COX inhibitor) abrogates the potentiated relaxation in AQP1 KO vessels (Fig. 10b, d) strongly supports causality for this enhanced COX-2 expression in the AQP1 KO vascular phenotype.

Table 4 Spectral analysis of systolic blood pressure (SBPV) or heart rate variability (HRV) in the very low frequency (VLF), the low frequency (LF), and the high frequency (HF) domains normalized to total spectral area (TS) in WT and AQP1 KO mice

	WT mice (n=16)	KO mice (n=13)	P value
VLF of SBPV/TS	0.235±0.005	0.237±0.004	ns
LF of SBPV/TS	0.281±0.012	0.29±0.018	ns
HF of HRV/TS	0.383±0.011	0.393±0.014	ns

Data are mean ± SEM

ns not significant compared to WT mice

Interestingly, the vessels of AQP1KO mice also exhibited characteristic morphometric differences, i.e., reduced wall thickness both in aorta and resistance (mesenteric) vessels. Whether this is a consequence or participates to the low systolic BP is unresolved. It is unlikely to simply be the consequence of low BP, since mice with endothelial-specific transgenic overexpression of eNOS, which exhibit 20 % lower systolic BP than their WT littermate (i.e., a more severe decrease in BP than our AQP1 KO mice), do not show any change in organ size or vessels morphology [31]. Rather, the morphometric changes observed here may in part be related to COX-2 overexpression, at least in resistance vessels. Indeed, genetic deletion of COX-2 resulted in severe pulmonary vascular smooth muscle cells (VSMC) hypertrophy (but no proliferation) and pulmonary hypertension in response to hypoxia, which could be reversed by exogenous PG(I2) or PG(E2), indicating a role for COX-2-derived prostanoids in the control of medial hypertrophy [11]. This does not exclude a direct implication of AQP1 as regulator of VSMC hypertrophy, as recently proposed [2] which would be in line with its expression across the vessel media.

Strikingly, AQP1 KO mice also exhibited a marked microcardia, as well as smaller cardiac myocytes cross-sectional area compared with WT littermates. Again, this is unlikely to merely be the consequence of the lower BP, since mice with even lower chronic hypotension do not exhibit a similar phenotype [31]. As we observed that these mice do not present permanent tachycardia compared to their littermate controls, lower stroke volume due to microcardia could at least in part contribute to their lower blood pressure. This microcardia is noteworthy in the context of the role of endothelial AQP1 in the process of cell migration involved, e.g., in angiogenesis [38], and previous demonstrations that physiologic cardiac development and hypertrophy are dependent on matching myocardial angiogenesis [41, 45]. However, we did not observe any decrease in capillary density (normalized per cardiac myocyte) that would support this hypothesis. Again, paracrine effects of COX-2-derived prostanoids from cardiac endothelium or a direct control of cardiac myocyte hypertrophy by AQP1 may be at play; for example, due to its strategic localization in cardiac cells within the T-tubules close to the Z line structure and in the associated vascular endothelium [10] and its osmolarity-dependent reversible internalization via caveolae [32], AQP1 could also modulate excitation contraction coupling requiring rapid osmotic equilibration. Failure to do so may perturb intracellular ion (e.g., calcium) homeostasis, with potential consequences on hypertrophic signaling although this needs to be tested in future experiments.

In conclusion, we found low systolic blood pressure with vessel and cardiac hypotrophy in AQP1 KO mice, together with upregulation of AQP7 in both tissues and AQP4 and AQP8 in the heart. Because of the proposed role of cardiac AQP1 (and AQP4) controlling the clearance of interstitial edema [9, 46, 47] and perhaps myocardial hypertrophic remodeling (this study), future studies will need to verify the specific effect of AQP1 deletion in pathological situations such as ischemia/reperfusion and pressure overload. Should an impact be observed, it may raise the interest for new modulators of AQP1 function derived from loop diuretics [8, 48] and their use to treat common situations, such as high blood pressure usually associated with hypertrophic cardiomyopathies.

Acknowledgments The authors are grateful to Yvette Cnops and Huguette Debaix from the Nephrology laboratory (NEFR/IREC), for their help in the RTqPCR and given some specifics primers for different aquaporins. VM is “Specialist doctorant” of the Fonds National de Recherche Scientifique (FNRS) and was supported by grants from the Fondation Saint Luc and FNRS (to JLB). CD is senior research scientist of the Fonds National de Recherche Scientifique (FNRS). CB is IREC imaging platform coordinator. These studies were supported in part by the European Community's Seventh Framework Programme (FP7/2007-2013) under grant no. 305608 (EURenOmics), the Actions de Recherche Concertées (ARC 10/15-029 and 11/16-039, Communauté Française de Belgique), the FNRS and FRSM, and the Inter-University Attraction Pole (Belgium Federal Government). The Aqp1 mice were initially obtained from A.S. Verkman (University of California, San Francisco, CA).

Ethical standards The experiments comply with the current laws of Belgium.

Conflict of interest The authors declare that they have no conflict of interest.

References

1. Agre P, Lee MD, Devidas S, Guggino WB (1997) Aquaporins and ion conductance. Science 275:1490
2. Al Ghouleh I, Frazziano G, Rodriguez AI, Csanyi G, Maniar S, St Croix CM, Kelley EE, Egana LA, Song GJ, Bisello A, Lee YJ, Pagano PJ (2013) Aquaporin 1, Nox1, and Ask1 mediate oxidant-induced smooth muscle cell hypertrophy. Cardiovasc Res 97:134–142
3. Beitz E, Wu B, Holm LM, Schultz JE, Zeuthen T (2006) Point mutations in the aromatic/arginine region in aquaporin 1 allow passage of urea, glycerol, ammonia, and protons. Proc Natl Acad Sci U S A 103(2):269–274
4. Butler TL, Au CG, Yang B, Egan JR, Tan YM, Hardeman EC, North KN, Verkman AS, Winlaw DS (2006) Cardiac aquaporin expression in humans, rats, and mice. Am J Physiol Heart Circ Physiol 291:H705–H713
5. Campbell EM, Birdsell DN, Yool AJ (2012) The activity of human aquaporin 1 as a cGMP-gated cation channel is regulated by tyrosine phosphorylation in the carboxyl-terminal domain. Mol Pharmacol 81:97–105
6. Denker BM, Smith BL, Kuhajda FP, Agre P (1988) Identification, purification, and partial characterization of a novel Mr 28,000 integral membrane protein from erythrocytes and renal tubules. J Biol Chem 263:15634–15642
7. Desjardins F, Lobysheva I, Pelat M, Gallez B, Feron O, Dessy C, Balligand JL (2008) Control of blood pressure variability in caveolin-1-deficient mice: role of nitric oxide identified in vivo through spectral analysis. Cardiovasc Res 79:527–536
8. Devuyst O, Yool AJ (2010) Aquaporin-1: new developments and perspectives for peritoneal dialysis. Perit Dial Int 30:135–141
9. Ding FB, Yan YM, Huang JB, Mei J, Zhu JQ, Liu H (2013) The involvement of AQP1 in heart oedema induced by global myocardial ischemia. Cell Biochem Funct 31:60–64
10. Egan JR, Butler TL, Au CG, Tan YM, North KN, Winlaw DS (2006) Myocardial water handling and the role of aquaporins. Biochim Biophys Acta 1758:1043–1052
11. Fredenburgh LE, Liang OD, Macias AA, Polte TR, Liu X, Riascos DF, Chung SW, Schissel SL, Ingber DE, Mitsialis SA, Kourembanas S, Perrella MA (2008) Absence of cyclooxygenase-2 exacerbates hypoxia-induced pulmonary hypertension and enhances contractility of vascular smooth muscle cells. Circulation 117:2114–2122
12. Gambert S, Helies-Toussaint C, Grynberg A (2005) Regulation of intermediary metabolism in rat cardiac myocyte by extracellular glycerol. Biochim Biophys Acta 1736:152–162
13. Gambert S, Helies-Toussaint C, Grynberg A (2007) Extracellular glycerol regulates the cardiac energy balance in a working rat heart model. Am J Physiol Heart Circ Physiol 292:H1600–H1606
14. Garcia F, Kierbel A, Larocca MC, Gradilone SA, Splinter P, LaRusso NF, Marinelli RA (2001) The water channel aquaporin-8 is mainly intracellular in rat hepatocytes, and its plasma membrane insertion is stimulated by cyclic AMP. J Biol Chem 276:12147–12152
15. He ZQ, Liang C, Wang H, Wu ZG (2008) Dysfunction of AQP7 in the periadventitial fat: a novel trigger of atherosclerosis. Med Hypotheses 70:92–95
16. Hennan JK, Huang J, Barrett TD, Driscoll EM, Willens DE, Park AM, Crofford LJ, Lucchesi BR (2001) Effects of selective cyclooxygenase-2 inhibition on vascular responses and thrombosis in canine coronary arteries. Circulation 104:820–825
17. Herrera M, Garvin JL (2007) Novel role of AQP-1 in NO-dependent vasorelaxation. Am J Physiol Ren Physiol 292:F1443–F1451
18. Herrera M, Garvin JL (2011) Aquaporins as gas channels. Pflugers Arch 462:623–630
19. Hibuse T, Maeda N, Nakatsuji H, Tochino Y, Fujita K, Kihara S, Funahashi T, Shimomura I (2009) The heart requires glycerol as an energy substrate through aquaporin 7, a glycerol facilitator. Cardiovasc Res 83:34–41
20. Hung KC, Hsieh PM, Hsu CY, Lin CW, Feng GM, Chen YS, Hung CH (2012) Expression of aquaporins in rat liver regeneration. Scand J Gastroenterol 47:676–685
21. Ishibashi K, Kondo S, Hara S, Morishita Y (2011) The evolutionary aspects of aquaporin family. Am J Physiol Regul Integr Comp Physiol 300:R566–R576
22. Kellen MR, Bassingthwaighte JB (2003) Transient transcapillary exchange of water driven by osmotic forces in the heart. Am J Physiol Heart Circ Physiol 285:H1317–H1331
23. Leggett K, Maylor J, Undem C, Lai N, Lu W, Schweitzer K, King LS, Myers AC, Sylvester JT, Sidhaye V, Shimoda LA (2012) Hypoxia-induced migration in pulmonary arterial smooth muscle cells requires calcium-dependent upregulation of aquaporin 1. Am J Physiol Lung Cell Mol Physiol 303:L343–L353
24. Ma T, Yang B, Gillespie A, Carlson EJ, Epstein CJ, Verkman AS (1998) Severely impaired urinary concentrating ability in transgenic mice lacking aquaporin-1 water channels. J Biol Chem 273:4296–4299
25. Ma T, Yang B, Verkman AS (1997) Cloning of a novel water and urea-permeable aquaporin from mouse expressed strongly in colon, placenta, liver, and heart. Biochem Biophys Res Commun 240:324–328

26. Maeng M, Olesen PG, Emmertsen NC, Thorwest M, Nielsen TT, Kristensen BO, Falk E, Andersen HR (2001) Time course of vascular remodeling, formation of neointima and formation of neoadventitia after angioplasty in a porcine model. Coron Artery Dis 12:285–293
27. Maunsbach AB, Marples D, Chin E, Ning G, Bondy C, Agre P, Nielsen S (1997) Aquaporin-1 water channel expression in human kidney. J Am Soc Nephrol 8:1–14
28. Moniotte S, Belge C, Sekkali B, Massion PB, Rozec B, Dessy C, Balligand JL (2007) Sepsis is associated with an upregulation of functional beta3 adrenoceptors in the myocardium. Eur J Heart Fail 9:1163–1171
29. Nagoshi T, Yoshimura M, Rosano GM, Lopaschuk GD, Mochizuki S (2011) Optimization of cardiac metabolism in heart failure. Curr Pharm Des 17:3846–3853
30. Ni J, Verbavatz JM, Rippe A, Boisdé I, Moulin P, Rippe B, Verkman AS, Devuyst O (2006) Aquaporin-1 plays an essential role in water permeability and ultrafiltration during peritoneal dialysis. Kidney Int 69:1518–1525
31. Ohashi Y, Kawashima S, Hirata K, Yamashita T, Ishida T, Inoue N, Sakoda T, Kurihara H, Yazaki Y, Yokoyama M (1998) Hypotension and reduced nitric oxide-elicited vasorelaxation in transgenic mice overexpressing endothelial nitric oxide synthase. J Clin Invest 102:2061–2071
32. Page E, Winterfield J, Goings G, Bastawrous A, Upshaw-Earley J (1998) Water channel proteins in rat cardiac myocyte caveolae: osmolarity-dependent reversible internalization. Am J Physiol 274:H1988–H2000
33. Pelat M, Dessy C, Massion P, Desager JP, Feron O, Balligand JL (2003) Rosuvastatin decreases caveolin-1 and improves nitric oxide-dependent heart rate and blood pressure variability in apolipoprotein E−/− mice in vivo. Circulation 107:2480–2486
34. Preston GM, Agre P (1991) Isolation of the cDNA for erythrocyte integral membrane protein of 28 kilodaltons: member of an ancient channel family. Proc Natl Acad Sci USA 88:11110–11114
35. Rojek A, Praetorius J, Frokiaer J, Nielsen S, Fenton RA (2008) A current view of the mammalian aquaglyceroporins. Annu Rev Physiol 70:301–327
36. Rutkovskiy A, Stenslokken KO, Mariero LH, Skrbic B, Amiry-Moghaddam M, Hillestad V, Valen G, Perreault MC, Ottersen OP, Gullestad L, Dahl CP, Vaage J (2012) Aquaporin-4 in the heart: expression, regulation and functional role in ischemia. Basic Res Cardiol 107:280
37. Saadoun S, Papadopoulos MC (2010) Aquaporin-4 in brain and spinal cord oedema. Neuroscience 168:1036–1046
38. Saadoun S, Papadopoulos MC, Hara-Chikuma M, Verkman AS (2005) Impairment of angiogenesis and cell migration by targeted aquaporin-1 gene disruption. Nature 434:786–792
39. Shanahan CM, Connolly DL, Tyson KL, Cary NR, Osbourn JK, Agre P, Weissberg PL (1999) Aquaporin-1 is expressed by vascular smooth muscle cells and mediates rapid water transport across vascular cell membranes. J Vasc Res 36:353–362
40. Skowronski MT, Lebeck J, Rojek A, Praetorius J, Fuchtbauer EM, Frokiaer J, Nielsen S (2007) AQP7 is localized in capillaries of adipose tissue, cardiac and striated muscle: implications in glycerol metabolism. Am J Physiol Ren Physiol 292:F956–F965
41. Tirziu D, Chorianopoulos E, Moodie KL, Palac RT, Zhuang ZW, Tjwa M, Roncal C, Eriksson U, Fu Q, Elfenbein A, Hall AE, Carmeliet P, Moons L, Simons M (2007) Myocardial hypertrophy in the absence of external stimuli is induced by angiogenesis in mice. J Clin Invest 117:3188–3197
42. Tradtrantip L, Tajima M, Li L, Verkman AS (2009) Aquaporin water channels in transepithelial fluid transport. J Med Invest 56(Suppl):179–184
43. Verkman AS, Yang B (1997) Aquaporins and ion conductance. Science 275:1491
44. Wakayama Y, Inoue M, Kojima H, Jimi T, Shibuya S, Hara H, Oniki H (2004) Expression and localization of aquaporin 7 in normal skeletal myofiber. Cell Tissue Res 316:123–129
45. Walsh K, Shiojima I (2007) Cardiac growth and angiogenesis coordinated by intertissue interactions. J Clin Invest 117:3176–3179
46. Warth A, Eckle T, Kohler D, Faigle M, Zug S, Klingel K, Eltzschig HK, Wolburg H (2007) Upregulation of the water channel aquaporin-4 as a potential cause of postischemic cell swelling in a murine model of myocardial infarction. Cardiology 107:402–410
47. Yan Y, Huang J, Ding F, Mei J, Zhu J, Liu H, Sun K (2013) Aquaporin 1 plays an important role in myocardial edema caused by cardiopulmonary bypass surgery in goat. Int J Mol Med 31:637–643
48. Yool AJ, Brown EA, Flynn GA (2010) Roles for novel pharmacological blockers of aquaporins in the treatment of brain oedema and cancer. Clin Exp Pharmacol Physiol 37:403–409
49. Yool AJ, Weinstein AM (2002) New roles for old holes: ion channel function in aquaporin-1. News Physiol Sci 17:68–72
50. Yu J, Yool AJ, Schulten K, Tajkhorshid E (2006) Mechanism of gating and ion conductivity of a possible tetrameric pore in aquaporin-1. Structure 14:1411–1423